

Biomaterials Science

Accepted Manuscript

This article can be cited before page numbers have been issued, to do this please use: V. L. Domingues Silva, A. Y. Kaassis, A. Dehsorkhi, C. Koffi, M. Severic, M. Abdelhamid, D. Nyimanu, C. J. Morris and W. Al-Jamal, *Biomater. Sci.*, 2020, DOI: 10.1039/C9BM01905G.



This is an Accepted Manuscript, which has been through the Royal Society of Chemistry peer review process and has been accepted for publication.

Accepted Manuscripts are published online shortly after acceptance, before technical editing, formatting and proof reading. Using this free service, authors can make their results available to the community, in citable form, before we publish the edited article. We will replace this Accepted Manuscript with the edited and formatted Advance Article as soon as it is available.

You can find more information about Accepted Manuscripts in the [Information for Authors](#).

Please note that technical editing may introduce minor changes to the text and/or graphics, which may alter content. The journal's standard [Terms & Conditions](#) and the [Ethical guidelines](#) still apply. In no event shall the Royal Society of Chemistry be held responsible for any errors or omissions in this Accepted Manuscript or any consequences arising from the use of any information it contains.

Enhanced selectivity, cellular uptake, and *in vitro* activity of an intrinsically fluorescent copper-tirapazamine nanocomplex for hypoxia targeted therapy in prostate cancer

Vera L. Silva¹, Abdessamad Kaassis^{1,2}, Ashkan Dehsorkhi¹, Cédrik-Roland Koffi², Maja Severic², Moustafa Abdelhamid¹, Duuamene Nyimanu^{1,3}, Christopher J. Morris¹, and Wafa' T. Al-Jamal^{1,2*}

¹*School of Pharmacy - University of East Anglia, Norwich Research Park, Norwich, NR4 7TJ, United Kingdom*

²*School of Pharmacy – Queen's University Belfast, Belfast, BT9 7BL, United Kingdom.*

³*Experimental Medicine and Immunotherapeutics, University of Cambridge, Centre for Clinical Investigation, Addenbrooke's Hospital, Cambridge, CB2 0QQ, United Kingdom.*

**Corresponding author*

Dr Wafa' T. Al-Jamal

School of Pharmacy

Queen's University Belfast

Belfast, BT9 7BL, United Kingdom

E-mail: w.al-jamal@qub.ac.uk

Abstract

In the present work, a copper-tirapazamine (TPZ) nanocomplex [Cu(TPZ)₂] was synthesized as a selective hypoxia-targeted therapy. The nanocomplex revealed a crystalline form, and exhibited higher lipophilicity, compared to TPZ. Furthermore, its stability was confirmed in different media, with minimum dissociation in serum (~20% up to 72 h). In contrast to other hypoxia-targeted agents, our intrinsically fluorescent nanocomplex offered an invaluable tool to monitor its cellular uptake and intracellular distribution under both normoxia and hypoxia. The conferred higher cellular uptake of the nanocomplex, especially under hypoxia, and its biocompatible reductive potential resulted in superior hypoxia selectivity in two prostate cancer (PC) cell lines. More promisingly, the nanocomplex showed higher potency in three-dimensional tumor spheroids, compared to TPZ, due to its slower metabolism, and probably deeper penetration in tumor spheroids. Interestingly, the nuclear localization of the intact nanocomplex, combined with its higher DNA binding affinity, as evidenced by the DNA binding assay, resulted in significant S- phase cell-cycle arrest, followed by apoptosis in three-dimensional spheroids model. In conclusion, the presented findings suggested that Cu(TPZ)₂ nanocomplex can be a promising hypoxia-targeted therapeutic, which could potentiate the efficacy of existing chemo- and radiotherapy in PC.

Introduction

Bio-reductive hypoxic activated pro-drugs (HAP) have been widely exploited as selective cytotoxic compounds, driven by low oxygen conditions, showing promise as novel cancer therapeutics^{1, 2}. Several *N*-oxide compounds have been proposed as potential candidates, with some progressing into clinical trials. Of particular interest is the hypoxic cytotoxin 3-amino-1, 2, 4-benzotriazine-1, 4-dioxide (tirapazamine – TPZ) which exhibits 30-300 times higher toxicity to cells in low oxygen conditions, compared to other cytotoxic agents³⁻⁵. TPZ is the most advanced bioreductive pro-drug in clinical trials, owing to its one-electron reduction pathway, and hypoxia selective DNA damaging action³. Nonetheless, its clinical efficacy has been limited by its poor cellular uptake, restricted tissue diffusion and rapid metabolism⁴.

Copper has attracted special attention over the last years as a promising metal coordinate to target cancer hypoxia. The low molecular weight, lipophilicity and planar structure of its complexes allow rapid cellular internalization and targeting of hypoxia^{6, 7}. It also possesses unique properties conferred by the variety of coordination geometries, metal-ligand interactions and redox activity that allows functionalization of ligands and effective cellular targeting (DNA, proteins, enzymes and redox pathways)⁸. Its unique electronic structure, and cell compatible reduction potential (E^0 ($\text{Cu}^{2+}/\text{Cu}^+$)) allows it to play a fundamental role in cellular growth and proliferation⁹. The coordination of metal ions to hypoxic cytotoxins is an interesting strategy to develop novel hypoxia-targeted therapeutics. These complexes have been exploited therapeutically with different organic ligands⁹, and in radiodiagnosis or radiotherapy¹⁰. Extensive work by J. Dearling, J. Holland and J. Dilworth has provided detailed analysis on the therapeutic and hypoxia imaging applications of copper-complexes^{7, 9-11}.

Copper-based complexes have now been widely exploited for anti-cancer therapy, and their potential thoroughly reviewed elsewhere¹². Most of these complexes presented improved chemical characteristics compared to the free ligand, contributing to their increased hypoxic uptake, thus more selective and/or potent biological activity^{11, 13-15}. Particular attention has been drawn to Cu(II) complexes including *N,N*-diimine ligands, thiosemicarbazones, bis(thiosemicarbazones), schiff base assemblies and pyridine-*N*-oxides and their ability to induce DNA damage, *via* binding or intercalation¹². Although this is the primary mechanism of action, new cellular targets such as DNA topoisomerases¹⁶, the proteasome complex^{17, 18}, endoplasmic reticulum¹⁹ and lysosome²⁰, have also become interesting pathways of cell death for copper-complex mediated therapeutics, highlighting the versatility and potency of these metal therapeutics.

Lin and Ho²¹ were the first to demonstrate the potential use of TPZ with copper to enhance DNA damaging in cancer cells. Next, they prepared a radioactive TPZ-copper complex for targeted cancer therapy²². These studies did not report the basic characterization of the complex, which, in our opinion, is

considered essential to further understand its biological relevance. Furthermore, data regarding its potential use as a hypoxia cytotoxic agent in more complexed hypoxia models is still warranted. In the present work, we aimed to synthesize and characterize a cupric-TPZ complex (abbreviated in the text as Cu(TPZ)₂). We sought to understand how complexation with copper could modulate TPZ's physicochemical properties (e.g. optical properties, solubility, and lipophilicity), and its biological activity. Ideally, this Cu(TPZ)₂ complex should maintain or improve TPZ hypoxia selectivity and potency while providing an innovative metal-complex strategy for hypoxia therapeutics. Therefore, it was essential to determine the selectivity and potency of this complex vs TPZ alone. Using both 2-dimensional (2D), and 3-dimensional (3D) prostate cancer models, the uptake and cytotoxicity of Cu(TPZ)₂ was determined in this study. Overall, Cu(TPZ)₂ complex should overcome some of the TPZ shortcomings *in vitro*, which could potentiate the efficacy of existing chemo- and radiotherapy *in vivo*.

Experimental

Materials

4-(2 Hydroxyethyl)piperazine-1-ethanesulfonic acid (HEPES), sodium chloride (NaCl), phosphate buffer saline (PBS) tablets, tirapazamine ($\geq 98\%$ HPLC), copper(II) chloride (97%), methanol (HPLC grade) and Universal MALDI Matrix [1:1, 2,5-dihydroxybenzoic acid (DHB): α -cyano-4-hydrocinnamic acid] were obtained from Sigma (UK). Laboratory reagent dimethyl sulfoxide (DMSO), chloroform (HPLC grade, stabilized with amylene), methanol (HPLC grade), and ethanol (absolute, 99.8%) were bought from Thermo Fisher Scientific (UK). Milli-Q water was prepared using a water purification system (Millipore Corp., Bedford, MA, USA). All organic solvents were of analytical grade, unless otherwise stated. All starting materials were commercially available research grade chemicals and were used without further purification.

Preparation of Cu(TPZ)₂ complexes

Two equivalents of TPZ (13.2 mg, 0.074 mmol) were added slowly to a total of 5 mL stirred ethanolic solution of CuCl₂ (5 mg, 0.037 mmol), resulting in the formation of a deep red precipitate. Following overnight stirring, the dark red precipitate was isolated, and washed with small volumes of ethanol by centrifugation at 5000 $\times g$ for 10 min, until a colorless supernatant was obtained. The red complex was then left to dry under vacuum at 25°C, and resuspended in DMSO until complete solubility was obtained (~ 2.5 mM stock solution). The complex was then sterile filtered through 0.2 μm membrane filter. The stoichiometry of the compound was [Cu(TPZ)₂], and the yield $\sim 70\%$ (11 mg, 0.026 mmol). The results of the elemental analysis (%) obtained with a Carlo Erba EA 1108 analyzer were: (C₁₄H₁₀CuN₈O₄) Found/Calcd.: C, 39.85/40.32; N, 25.66/26.87; H, 2.39/2.21. IR (ATR) analysis: (ν/cm^{-1}) - ($\nu_{\text{N-H}_2}$), 3360-3311; ($\delta_{\text{N-H}_2}$), 1570; ($\nu_{\text{N} \rightarrow \text{O}}$), 1358; ($\nu_{\text{C-N}}/\nu_{\text{C-C}}$), 1111, 1165, 1215. MALDI-MS: m/z (%) [Cu(TPZ)₂-H]⁺, Found/Calcd (%): 418.0199/418.0202 (100). Full details of TPZ and Cu(TPZ)₂ characterization can be found in the experimental section of the supplementary information.

Biological studies

In vitro cytotoxicity of TPZ and Cu(TPZ)₂ complex in PCa monolayers

LNCap (CRL-1740™) and C4-2B cells were purchased from ATCC® and MD Anderson Cancer Center (Texas, USA), respectively. The cells were maintained in Advanced RPMI-1640 (1x) medium supplemented with 10% heat inactivated FBS, 1% penicillin/streptomycin and 1% GlutaMax (200 mM). Cells were maintained in Corning® CellBIND® 75 cm³ canted-neck tissue culture flasks (Fisher Scientific, UK) to enhance cell adherence. For normoxic condition, cell cultures were maintained in a humidified incubator at 37°C in 5% CO₂/95% air. For hypoxia treatment, cells were placed in a hypoxic chamber (Incubator chamber Billups Rothenberg Inc., MIC-101) with a mixture of 1% O₂, 5% CO₂, and 94% N₂ (BOC, UK). Hypoxia was validated using the CYTO-ID® Hypoxia/Oxidative Stress Detection kit (Enzo Life Sciences, UK) according to the manufacturer manual²³.

Cell culture media and drug stock solutions were pre-purged with the hypoxic gas mixture to minimize oxygen fluctuations. The cytotoxicity of TPZ and Cu(TPZ)₂ was determined using the resazurin assay, as previously described²⁴. Resorufin fluorescence intensity (FI) was measured using a BMG microplate reader (FLUOstar Omega, BMG Labtec) at 544 nm excitation and 590 nm emission. The average percentage cell viability was calculated by normalizing the values to the untreated cells, using the following formula:

$$\text{Cell Viability (\%)} = \frac{\text{FI}_{\text{treated}}}{\text{FI}_{\text{control}}} \times 100$$

Uptake and cellular localization of TPZ and Cu(TPZ)₂ complex

For quantitative uptake studies, confluent C4-2B cells were harvested by trypsinization and seeded onto pre-coated poly-D-lysine (100 µg/mL) 24 flat-bottom well plates (Triplered, UK) at 5 × 10⁴ cells/well. The cells were incubated overnight under either normoxia or hypoxia to allow adherence. Next, cells were incubated with free TPZ or its complex (100 µM equivalent TPZ) at 37 °C for 1, 4, 8 and 24 h to assess uptake. At specific time periods, the medium was removed and the wells were washed (3X) with 200 µl of cold PBS to remove any free drug. After that, cells were harvested by trypsinization and pelleted by centrifugation (500 × g, 10 mins). The pellet was resuspended in 200 µL of DMSO (to guarantee solubility of released drug) and cells were then lysed by mechanical disruption using a bath sonicator for about 15 min (Ultrasound cleaning baths, USC, VWR). This ensured full disruption of cell membrane and intracellular organelles. The fluorescence intensity of each sample well was measured using a microplate reader (FLUOstar Omega, BMG Labtec) at 485 nm excitation and 590 nm emission. The percentage of drug uptake was calculated by dividing the fluorescence of each well by the fluorescence of the initial drug concentration used.

For fluorescence microscopy, C4-2B cells were seeded at 5 × 10⁴/well onto pre-coated poly-D-lysine (100 µg/mL) Coverslips (Fisher Scientific, UK), placed in 24 well assay plates (Triplered,

UK) and left to adhere overnight at 37 °C under normoxia or hypoxia. Next, the cells were incubated with TPZ or its complex for 1, 4, 8 and 24 h, under both normoxia or 1% hypoxia. Cells were then washed with cold PBS and fixed with 4% PFA at room temperature for 20 min, then washed (3X) with cold PBS. The nuclei were stained with Hoechst 33258 (5 µg/mL) (Sigma, UK) for 30 min at 37°C. Finally, the coverslips were washed (3X) with PBS, and mounted using ProLong™ Gold Antifade mounting media (Fisher Scientific, UK). Images were obtained using a Zeiss Axioplan 2 epifluorescence Axiovision 4.1.8 software. Images were processed and analysed using ImageJ (NIH, Bethesda, MD, USA: <http://imagej.nih.gov/ij>). For each endpoint, duplicates of two independent experiments (n=2) resulted in the analysis of over 50 cells. For some experimental conditions a z-stack with 1.75 µm intervals was generated using the Apotome to form a 3D reconstruction and evaluate co-localization *via* orthogonal projections. All images were acquired with a 10x/0.45 air objective and Axiovision 4.1.8 software, processed and analysed using ImageJ (NIH, Bethesda, MD, USA: <http://imagej.nih.gov/ij>).

Analysis of Cu(TPZ)₂ metabolism using FTIR and NMR

C4-2B cells were seeded on pre-coated poly-D-lysine (100 µg/mL) at 5 × 10⁴/well in 24 well assay plates (Triplered, UK) and left to adhere overnight at 37 °C under hypoxia. Next, the cells were incubated with TPZ in its free or complex form (100 µM equivalent TPZ) for 1, 4, 8 and 24 h, under 1% hypoxia using a hypoxic chamber (Ruskin Invivo2 400 Hypoxia Workstation). At specific time periods, the medium was removed and the wells were washed (3X) with PBS to remove any free drug, and cells were lysed with 200 µL of RIPA buffer. Cell lysate samples were stored at -20 °C until further FTIR and NMR analysis.

200 µL of cell lysates was diluted in 200 µL D₂O (Fisher, UK) and probed by nuclear magnetic resonance (NMR). The Spectra were recorded at 297 K, on an ultra-shield 400 instrument (¹H frequency: 400 MHz; Bruker, Germany). Then, all the samples were dried and were dissolved in 400 µL CDCl₃ in presence of Tetramethyl silane (TMS) and run at the same conditions. Finally, the samples were dried and dissolved in DMSO in the presence of TMS. The samples were analyzed using IR spectroscopy (Spectrum Two FTIR, Perkin Elmer, USA) over the range 650–4000 cm⁻¹ with a resolution of 4 cm⁻¹.

In vitro cytotoxicity of TPZ and Cu(TPZ)₂ in C4-2B spheroids

C4-2B spheroids were cultured and characterized as described in the supporting information. Five days post spheroid seeding, 100 µL of media was carefully removed and replaced with pre-diluted fixed concentrations of TPZ in free and complexed form (TPZ equivalent: 0.002 up to 20 µM). Spheroids were treated for 48, 72 and 96 h using 10% DMSO as a positive control. Spheroids were carefully washed with PBS 1x and replenished with fresh media or pre-treated with EDTA (5 mM) for 30 min, with shaking (70 rpm) to ensure resazurin penetration and reliable quantification²⁴. Resazurin solution (20 µl) was then added to each well and the spheroids were further incubated overnight, at 37°C to determine cell viability. To complement the viability assay, representative spheroid images were taken to monitor spheroid size changes before and after treatment. The average percentage cell viability for each drug concentration was expressed as mean ± S.D of six replicates of

three independent experiments (≥ 18 spheroids, $n \geq 2$) and calculated by normalizing the FI values to the untreated cells. Dose-response curves were generated, where possible, and the IC_{50} values for drug inhibition were determined by nonlinear regression analysis of the data fit to a four-parameter equation (GraphPad Prism version 7, La Jolla California USA www.graphpad.com).

Cell cycle and apoptosis analysis using Flow Cytometry

C4-2B spheroids were cultured at a density of 5×10^3 cells/well, as described above and on day 5 of growth, were treated with 2 and 20 μM (equivalent TPZ content) in free and copper-complexed form. Untreated spheroids were used for population gating to avoid the undesired noises from debris and singlet gating to minimize debris and cell aggregates. 72 h post-treatment, spheroids were harvested, using a 1 mL pre-cut micropipette tip, into 1.5 mL micro centrifuge tubes (Fisher Scientific, UK) and centrifuged at $500 \times g$ for 5 min, to sediment the spheroids. The cells were then washed $3 \times$ with cold PBS, with repeated centrifugation and resuspended in 100 μL of PBS. Thereafter, a single cell suspension was formed by mechanical dissociation, using a micropipette, and cells were fixed in 70% ethanol for at least 1 h, on ice. To achieve this, 400 μL of ice-cold 70% ethanol was added dropwise to each sample, while vortexing to ensure complete fixation and avoid cell clumping. Cells were then washed $3 \times$ with PBS (first spin at $800 \times g$, 10 min, to recover all cells) and the cell pellet was resuspended in 0.5 mL of propidium iodide/RNase solution (FxCycle™ Solution, Molecular Probes, UK). The samples were incubated for 30 min at room temperature, protected from light and further analysed, without washing, by flow cytometry using a Becton Dickinson CytoFLEX (Beckman Coulter, UK). Cell doublets were separated from single cells in G2/M phase using pulse-width/pulse-area signal. At least 10,000 cells were acquired in a histogram and cell cycle data were exported as FSC files and analysed using FlowJo software. Each data measurement was made up from at least ten pooled spheroids, repeating the whole procedure independently two times ($n=2$). Results were expressed as mean \pm S.D, after population deconvolution, peak integration and calculation of population percentage.

DNA binding studies

The interaction between $\text{Cu}(\text{TPZ})_2$ (25 μM) and calf-thymus DNA (CT-DNA) was analysed by UV/Vis spectroscopy. The CT-DNA stock solution, was prepared in Tris-buffer (containing 5 mM Tris-HCl and 50 mM NaCl at pH 7.2). The UV absorbance at 260 and 280 nm of the CT-DNA gave a ratio of 1.84, indicating that DNA was sufficiently free of protein contamination. DNA stock concentration (8.71 mM) was determined spectrophotometrically at 260 nm, by using the molar extinction coefficient value of $6600 \text{ M}^{-1} \text{ cm}^{-1}$.²⁵

$\text{Cu}(\text{TPZ})_2$ (25 μM) solutions were also prepared in Tris-buffer, where red dispersion was observed, indicating good dispersion of the complex in this buffer. We further performed electronic absorption titrations, which were carried out with a constant concentration of the copper(II) complex (25 μM) and varying concentrations of CT-DNA (0–500 μM) in Tris-buffer. The complex and DNA solutions were incubated at 37 $^\circ\text{C}$ for 24 h. Subsequently, the spectra were recorded using a UV/Vis spectrophotometer at ambient temperature. Solutions of free CT-DNA (namely in the absence of copper compound) at the

corresponding concentrations (0–500 μM) were used as blanks before recording the absorption band of each sample. The titrations of the corresponding concentration of TPZ (50 μM) were also performed, with varying concentrations of CT-DNA (0–500 μM). Solvent samples without DNA or drug were used as baseline references. The results were presented as mean absorbance of triplicate samples of two independent experiments ($n=2$).

The intrinsic binding constant (K_b) for the interaction of $\text{Cu}(\text{TPZ})_2$ with CT-DNA was calculated using the following equation:

$$\frac{[\text{DNA}]}{\epsilon_a - \epsilon_f} = \frac{[\text{DNA}]}{\epsilon_b - \epsilon_f} + \frac{1}{K_b (\epsilon_b - \epsilon_f)}$$

where ϵ_a , ϵ_f and ϵ_b correspond to, the apparent molar extinction coefficient - $A_{\text{obsd}}/[\text{Cu}]$, the molar extinction coefficient for the free $\text{Cu}(\text{TPZ})_2$, and the molar extinction coefficient for the $\text{Cu}(\text{TPZ})_2$ in the fully bound form, respectively. By plotting $[\text{DNA}]/(\epsilon_a - \epsilon_f)$ vs $[\text{DNA}]$, K_b was then determined by calculating the ratio of the slope to the intercept.

Statistical analysis

Data was presented as mean \pm SD. Two-way Analysis of variance (ANOVA) and Bonferroni multiple comparisons post-hoc test was performed when three or more groups of data were analysed. P-values < 0.05 were considered significant and statistical differences amongst groups was appropriately denoted in the figure captions. The IC_{50} values for inhibition were determined by nonlinear regression analysis of the data fit to a four-parameter equation. All analyses and graphs were generated using GraphPad Prism version 7.0 (GraphPad Software, La Jolla California USA, www.graphpad.com).

Results

$\text{Cu}(\text{TPZ})_2$ synthesis and characterization

In this study, $\text{Cu}(\text{TPZ})_2$ complex was prepared by mixing TPZ with CuCl_2 salt in an ethanolic solution (Figure. 1A). The red precipitate was collected, and its chemical structure was confirmed using elemental analysis, FTIR (Figure. S1), and mass spectrometry (MS) (Figure. S2). The relevant physicochemical properties (molecular mass, pKa and logP values) of TPZ²⁶ and $\text{Cu}(\text{TPZ})_2$ ²⁷ were summarized in Figure. 1B. Based on the literature, $\text{Cu}(\text{TPZ})_2$ complex exhibited a biocompatible reductive potential (-0.75V vs. Ag/AgCl), which was more electronegative than that presented by TPZ (-0.65V vs. Ag/AgCl), suggesting superior selectivity under hypoxia^{10, 19, 20, 28}.

The morphology and the structure of the isolated $\text{Cu}(\text{TPZ})_2$ complex were also analyzed using TEM and X-ray powder diffraction (XRD), respectively. Due to the higher hydrophobic nature of the complex (solubility $\sim 2.5 \text{ mM}$ in DMSO), some intermolecular interactions occurred at high concentrations, resulting in highly organized nanostructures in more polar

solvents (e.g. ethanol). Interestingly, TEM examination revealed that the complex morphology was concentration-dependent, where needle-like structures (300-400 nm in length) were present at high concentrations (2 mM), and tiny and homogenous spherical nanoparticles (3-4 nm in diameter) were observed at lower concentrations (20 μ M) (**Figure. 1C**), similar to the concentration range used in this study (20 μ M). The large needle structures possibly result from $\pi \rightarrow \pi$ stacking and van der Waals interaction between molecules^{14, 17}, which strongly agrees with the proposed 3D structure (**Figure. 1A**). Single-crystal X-ray diffraction measurement was not possible to perform due to the small size of the complex crystals, however, the XRD result confirmed that the complex is in the crystalline form, with the following diffraction reflections 8.3 $^\circ$, 10.9 $^\circ$, 13.4 $^\circ$, 15.6 $^\circ$, 18.9 $^\circ$, 25.6 $^\circ$ and 28.7 $^\circ$ (**Figure. S4**). All the complex characterization results are described in detail in the supporting information.

Cu(TPZ)₂ stability and dissociation in different media

TPZ complexation was further confirmed using UV-Vis spectrophotometry. Both free and complexed TPZ showed similar optical properties in DMSO, with two characteristic absorption peaks at λ_{\max} 280 nm and 500 nm (**Figure. 1D**). In HBS TPZ presented a less intense band at λ_{\max} 280 nm and a more intense band at λ_{\max} 462 nm (**Figure. 1E**), arisen from the $\pi \rightarrow \pi^*$ transitions in the phenyl group and $\pi \rightarrow \pi^*$ transitions from the pyridine-*N*-Oxide, respectively. Cu(TPZ)₂ maintained a ligand centered band at λ_{\max} 280 nm and a broad absorption band in the visible region at 500-600 nm, which is characteristic for copper (II) d-d transition band (band I: $d_{xy,yz} \rightarrow d_{x^2-y^2}$)²⁹. The optical properties in different aqueous media were also studied, as described in the supporting information (**Figure. S5**).

To fully understand the dissociation mechanism of the complex, a simple titration study was performed by diluting the formed complex in aqueous buffers with a wide range of pH (**Figure. 1F**). An immediate color change was observed by decreasing the pH from 7.4 to 5. This was confirmed by a visible shift in the complex absorption (555 nm and 595 nm) to a lower wavelength (462 nm), indicating the dissociation of the complex at lower pH. A single sigmoidal curve was fitted to the absorbance at 462 nm and plotted against pH, providing a pKa value of 2.7 (**Figure. S5D**), comparable to that obtained before for TPZ²⁷. Furthermore, the stability of the complex was assessed in 50% serum, where minimum dissociation was evidenced (~20% up to 72 h) (**Figure. S6**), indicating high stability of the complex under physiological conditions. It is possible that a small number of Cu(TPZ)₂ molecules could have undergone copper-translocation *via* serum albumin⁴⁷, leading to free TPZ liberation.

Cellular uptake and metabolic analysis of intrinsically fluorescent Cu(TPZ)₂ complex

Poole *et al.* previously reported weak fluorescence of TPZ in solutions³⁰. This agrees with our findings, where TPZ was fluorescent a wide range of aqueous media (**Figure. S7A**), except at pH 12.5 (**Figure. S7B**)³⁰. Our current results showed that complexing TPZ to copper did not affect TPZ fluorescence emission in DMSO (**Figure 2A, left**). On the other hand, a significant enhancement in intensity was observed in HBS buffer pH 7.4 (**Figure. 2A, right**), with a 50-nm red shift upon

coordination to the metal center. Interestingly, as the complex dissociated at low pH, a two-fold reduction in the fluorescence intensities was observed, reaching the same level of free TPZ. This strongly indicates that the fluorescent enhancement was metal-induced (**Figure. S7C**). Despite the strong quenching capacity of Cu(II), such fluorescence enhancement following copper complexation was previously reported²⁸.

Encouraged by the intrinsic fluorescence of the complex, and its high serum stability, we further monitored its cellular localization and accumulation under normoxia (21% O₂) and 1% hypoxia, where the latter was validated using a hypoxia marker (**Figure. S8**). Representative images were then taken at 1, 4, 8 and 24 h under normoxia (**Figure 2B, left**) and hypoxia (**Figure 2B, right**), which showed the cellular accumulation of Cu(TPZ)₂ (green fluorescence) in C4-2B cells. Interestingly, the results depicted a rapid uptake (1 h) of the complex, with strong green fluorescent signals in the cytosol and perinuclear region, under both normoxia and 1% hypoxia. Furthermore, some images evidenced nuclear localization of the intact fluorescent complex, presented as diffuse green signals in the nucleus (**Figure 2B**) or as punctate signals (**Figure. S9**). At 4 h, the appearance of bright green punctate structures (depicted by white arrows), particularly in hypoxic conditions, suggested that copper complex can also accumulate in lysosomal compartments or autophagic structures^{6, 10, 11, 14}, however, the exact mechanism of the complex internalization should be confirmed. After 8 h, the fluorescent signals were clearly lower, suggesting complex efflux, dissociation or metabolism, as we further confirmed. A slight increase in fluorescence was observed after 24 h, possibly due to reoxidation of a small number of Cu(TPZ)₂ molecules *via* copper recycling pools. Further studies are required to investigate this observation.

TPZ's weak fluorescence was not reliable to evaluate its cellular uptake and localization under the same conditions (**Figure. S10**). Therefore, we developed a quantitative method to assess the complex uptake overtime. We compared the total uptake of TPZ and Cu(TPZ)₂, up to 24 h, under both normoxia and 1% hypoxia conditions (**Figure. 2C**). As evidenced before⁵, TPZ showed low cellular uptake, with no significant differences under both normoxia and hypoxia. On the other hand, Cu(TPZ)₂ showed a significant improvement in cellular uptake, under normoxia (4 h, $p < 0.001$; 8 h, $p < 0.01$ and 24 h, $p < 0.0001$) and hypoxia (4 h, $p < 0.0001$; 8 h, $p < 0.05$ and 24 h, $p < 0.0001$), compared to TPZ (**Figure. 2C**). These observations could be attributed to the higher lipophilicity of the complex (LogP 2.88) compared to TPZ (LogP -0.31). More importantly and in line with previous reports^{10, 13, 14}, the complex demonstrated selective hypoxia uptake at 4 h with higher uptake efficiency compared to normoxia ($p < 0.001$). The bio-reductive cycle in the lysosome ($E_{\text{red}} -0.75$), could be responsible for this high intracellular accumulation, with decreased complex efflux under hypoxia¹⁵. The full mechanism underlining this hypoxia selectivity is detailed in the discussion section. Furthermore, the slight decrease in cell uptake at 8 h, could be attributed to complex dissociation in acidic compartments, such as lysosomes, with consequent loss of fluorescence intensity, which agrees with the fluorescent imaging and previous results (**Figure S7C**).

Drug metabolism could be responsible for the decreased intracellular concentrations of the complex. To verify this, we assessed the metabolism of TPZ and the complex following cell internalization, under hypoxia, using non-fluorescent-based techniques, namely FTIR and NMR. Our qualitative FTIR results, revealed a fast metabolism of TPZ, in contrast to the complex, where free TPZ was metabolized and an intermediate was formed within 1 h of cell internalization (Figure. S11). This fast TPZ metabolism is in agreement with the literature³¹. On the other hand, neither free TPZ, nor its intermediate metabolite was detected in the cell lysate samples incubated for 1 h with the complex (Figure. S12), re-emphasizing the stability of the complex intracellularly, and its slow metabolism, respectively. Between 4 and 24 h similar metabolites were present in all samples. Moreover, as anticipated, the metabolite levels in the TPZ samples were much higher compared to cells incubated with the complex (Figure. 3C), indicating slower metabolism of the complex, as confirmed by NMR. These quantitative results showed that the levels of the complex metabolites, in contrast to free TPZ, fluctuated over time, with the highest level detected after 4 h. The metabolism decreased slightly around 8 h, before increasing again after 24 h (Figure. 3C). It is worth mentioning that the complex was present in the cell lysate (pellet) samples (Figure. 3B), but could not be detected using NMR, since it was precipitated from the supernatant due to a solubility issue. Interestingly, these results could justify the loss of fluorescence signal at 8 h (Figure. 2B& 2C), followed by some signal recovery at 24 h. Several *in vitro* studies reported TPZ benzotriazine radical and mono-*N*-oxide (SR4317) as major TPZ metabolites³², however, in presence of DNA, identifying the exact metabolites becomes more challenging, since the interaction of TPZ benzotriazine radicals with the DNA results in DNA damage, and different products are formed³³. The latter observation could possibly explain the unreported metabolite peaks detected by NMR (Figure. 3), however, the exact metabolites formed in our study remain to be identified.

Hypoxia selectivity of Cu(TPZ)₂ complex in PCa cells

To assess hypoxia selectivity, the cytotoxicity of free TPZ and Cu(TPZ)₂ complex was studied under normoxia (21% O₂) and 1% hypoxia in two prostate cancer (PCa) cell lines. The inhibitory concentrations (IC₅₀) were determined under both conditions and used to calculate the hypoxia cytotoxicity ratio (HCR, IC₅₀ normoxia/IC₅₀ hypoxia), which expresses hypoxia selectivity. The IC₅₀ and HCR values obtained in the PCa cell lines are summarized in Table S1.

Our results demonstrated that the cytotoxicity of TPZ and its complex was cell-, and time-dependent (Figure. 4A). C4-2B, an androgen-independent³⁴, derived bone metastatic PCa cell model, exhibited high sensitivity to the hypoxia pro-drugs, with clear dose-response shifts to the left at 1% hypoxia (Figure. S13). The effect was especially pronounced in terms of hypoxia selectivity, confirmed by the overall increased HCR values of Cu(TPZ)₂, compared to TPZ (Table S1). The HCR values were consistently higher for the complex and achieved exceptional selectivity for this cell line at 72 h post-treatment (HCR: 72 h, ~70). Furthermore, the cytotoxic effects under normoxia revealed a significant 2.03, 2.61 and 3.78-fold increase in IC₅₀ (at 48, 72 and 96 h, respectively) for Cu(TPZ)₂ compared to TPZ alone (Figure. 4A, top panel). More promisingly, enhanced potentiation of the complex under hypoxia (IC₅₀: 1.61 ± 1.0),

compared to TPZ (IC₅₀: 2.831 ± 1.04 μM) was also obtained at 72 h time-point, confirming the augmented selectivity and therapeutic potency of the complex in C4-2B. Similar findings were obtained in LNCap, an androgen-dependent PC cells (Figure. 4A, bottom panel), which showed high sensitivity to both agents under hypoxia (Figure. S14), and superior hypoxia selectivity with the Cu(TPZ)₂ (Table S1). LNCap cells have been shown to readapt under hypoxia, through a metabolic shift, which may sensitize these cells to hypoxia-selective treatments³⁵. It is therefore plausible to argue that oxygenation is only one parameter influencing the activity of these drugs and may well be a simplistic view of their MoA. All cell lines were cultured under the same conditions, yet they exhibit differences in toxicity and selectivity. Hypoxia adaptation and the reductive capacity of these cell lines will certainly influence the sensitivity to TPZ and Cu(TPZ)₂.

Potency of Cu(TPZ)₂ against C4-2B tumor spheroids

In order to validate the previous cytotoxicity data in monolayers, 3D hypoxia models of C4-2B, were developed (Figure. 5A & Figures. S15-S16), and C4-2B spheroids were incubated with TPZ or Cu(TPZ)₂ up to 96 h. The resazurin assay was used to quantify cell viability, and spheroids imaging was used to monitor cell morphology post-treatment (Figure. S17). As expected, TPZ (Figure 5B) was less potent in spheroids (Table S2) compared to C4-2B monolayers (Table S1). Furthermore, TPZ toxicity in 3D cultures was not dose- or time-dependent (IC₅₀: 48h, 35.17 ± 1.17 μM; 72h, 26.21 ± 1.18 μM, 96h: 36.02 ± 1.89 μM) (Figure. 5B & Table S2). This data indicated that TPZ's toxicity is possibly restricted to the spheroid surface layer, since it is metabolized too rapidly^{26, 31, 36-39}, as we previously showed. On the other hand, Cu(TPZ)₂ showed dose and time-dependent cytotoxicity in C4-2B spheroids (Figure 5C and Table S2) (IC₅₀: 48h, 41.78 ± 5.67 μM; 72h, 25.58 ± 3.78 μM, 96h: 13.33 ± 1.43 μM). The results correlated well with the different metabolic rates of the complex compared to TPZ (Figure. 3). At 48 h, spheroids were slightly more resistant to Cu(TPZ)₂ (IC₅₀: 41.78 ± 5.67 μM) compared to TPZ (IC₅₀: 35.17 ± 1.17 μM), but reached a pronounced therapeutic activity at 96h (Cu(TPZ)₂, IC₅₀: 13.33 ± 1.43 μM; TPZ, IC₅₀: 36.02 ± 1.89 μM, p<0.0001).

Furthermore, in order to determine the cellular responses after TPZ and Cu(TPZ)₂ drug testing, cell cycle and apoptosis analyses were carried out. 5-days post seeding, C4-2B spheroids were treated for 72 h with 20 and 2 μM equivalent TPZ in both free and complex forms. Cell cycle histograms were generated to evaluate cell cycle distribution (Figure. S18). Interestingly, data showed marked arrest in S-phase population, followed by decrease in G1 for Cu(TPZ)₂ treated spheroids at both 10 (p<0.05) and 1 μM (p<0.01), compared to untreated or TPZ-treated spheroids (Figure. 5D). Furthermore, this significant S-phase arrest was accompanied by increased propidium iodide (PI)-positive apoptotic cells following Cu(TPZ)₂ (10 μM) treatment, compared to untreated and TPZ groups (Figure. 5E).

Enhanced DNA binding of Cu(TPZ)₂

The cell cycle analysis results suggested that TPZ cytotoxicity in C4-2B spheroids may be mediated by non-selective mitochondrial and ROS induced cell death⁴⁰, while Cu(TPZ)₂ may exert an increased DNA selective cytotoxic activity. To

confirm the latter, UV–Vis absorption spectra of free TPZ were recorded in the absence and presence of increasing concentrations of CT-DNA solution (Figure. 5F). No spectral changes were observed, indicating that TPZ did not interact with DNA in the absence of its radical counterpart⁴¹. On the other hand, Cu(TPZ)₂ (Figure. 5G) showed a significant hyperchromic effect in the entire spectrum, with a small bathochromic shift, which indicates a non-intercalative binding mode through DNA groove binding, resulting in damaging of the DNA double-helical structure²⁵. The DNA binding constant (K_b , $0.18 \times 10^2 \text{ M}^{-1}$) (Figure. 5G, inset), was in agreement with other DNA groove binding agents and much lower than standard DNA intercalators⁴². This indicates that Cu(TPZ)₂ complex has a moderate DNA binding capacity, possibly through DNA groove binding, but intercalation cannot be ruled out, supporting previous evidence on the enhanced DNA damaging capacity of this complex²¹. Further studies on DNA viscosity, damage and ROS production can further elucidate the mechanisms of action of this cupric-TPZ complex.

Discussion

Cancer hypoxia has been highly associated with treatment resistance and metastasis; therefore, a wide range of hypoxia-activated prodrugs have been developed to targeting hypoxia^{1, 2}. TPZ is the most advanced bioreductive pro-drug in clinical trials, however, its clinical efficacy has been limited by its poor cellular uptake, restricted tissue diffusion and rapid metabolism⁴. Several structure-activity relationship (SAR) studies with TPZ analogues have provided substantive correlation between specific substituents (and their position) with improved pharmacological outcomes⁴³. Moreover, the use of transition metal complexes has shown to be a particularly suitable strategy to modify existing pro-drugs and develop a new biologically active molecule with improved hypoxia activity⁷. Copper(II) complexes have shown to coordinate well with 1,2,4-benzotriazine 1,4-di-*N*-oxides^{44, 45}, generating prodrug complexes that are stable under physiological conditions, but become kinetically labile with changes in the redox status or pH of the environment. Two studies reported TPZ-copper complex as a hypoxia-selective agent in 2D culture^{21,22}, however, these studies neither demonstrated any correlation between the complex characteristics and its biological activity, nor assessed its activity in 3D hypoxia culture models. In our work, we have revealed unreported characteristics of the complex, such as its lipophilicity (LogP 2.88), particulate nature, slow metabolism, as well as its superior intrinsic fluorescence, enabling its cellular trafficking and quantification under normoxia and hypoxia. Collectively, with the published reductive potential of the complex, we have been able, and for the first time, to provide better understanding of the biological activity of the complex in 2D and 3D hypoxia PC models.

TPZ has been shown to possess a pH-dependent cytotoxicity⁴⁶, where the slightly acidic microenvironment (pH 6.0) dramatically increased its aerobic cytotoxicity, thus contributing to the observed clinical side-effects (muscle cramping, peripheral neuropathy, and intestinal symptoms)^{4, 5}. Interestingly, our results suggest that the high pH stability of the complex could minimize TPZ systemic toxicity. Studies have also shown that the reductive hypoxic environment plays a key role in determining the dissociation rate of metal-

complexes. Previous reports have shown that copper trans-chelation could occur with serum albumin^{14, 39, 40}, or thiol-rich molecules (glutathione, cysteine and ascorbate), which are capable of reducing these complexes intracellularly²⁷. The former was not observed with our complex since high serum stability was observed. Nevertheless, previous data²¹ showed that TPZ can compete with glutathione for copper, but not EDTA, once again confirming the stability of Cu(TPZ)₂. All these findings are important from a biological point of view, and the data presented here suggested that Cu(TPZ)₂ may be dissociated *via* a pH-dependent mechanism, intracellular thiol-mediated reduction, but not by serum albumin trans-chelation emphasising its stability in the blood following its systemic administration.

Previous reports, have shown high potentiation of TPZ under different hypoxia levels (HCR: 30-300) that was cell-line dependent⁴. Factors such as p53 status, expression of reductive enzymes, *e.g.* cytochrome c P450⁴⁸, CA-IX, acidic microenvironment and of homologous recombination proteins (XRCC2, Rad51D, BRCA1 and BRCA2) have been shown to influence TPZ sensitivity and cannot be ruled out⁴⁸. Interestingly, the PC cell lines used here showed differential metabolic profiles under hypoxia and aggressiveness is marked by defects in DNA repair mechanisms, p53 status and increased basal ROS levels³⁵. Previously, Adsule *et al.*¹⁸, developed a potent quinoline-2-carboxaldehyde copper complex, which inhibited proteasome activity in PC-3 and LNCaP cells (IC₅₀ of 4 and 3.2 μM, respectively). However, studies were only carried out under normoxic conditions, not specifying any hypoxia selectivity. In this work, Cu(TPZ)₂ complex exhibited low cytotoxicity under normoxia with IC₅₀ above *ca.* 50 μM for all cell lines, while under 1% hypoxia IC₅₀ values ranged from moderate (>10 μM) to potent activity (<10 μM). Cu(TPZ)₂ showed higher potency, compared to TPZ, in C4-2B, but higher selectivity was observed in both cells tested. The HCR heatmap results (Figure. 4B) showed a moderate effect at 48 h, for both drugs, against LNCaP, and C4-2B. HCR values were consistently higher for Cu(TPZ)₂ (>10) in LNCaP and C4-2B, compared to TPZ, with outstanding selectivity in C4-2B after 72 h (HCR of *ca.* 70), confirming the potential of this complex as HAPs in PC. This superior selectivity is attributed to the higher electronegativity of the complex compared to TPZ. Most research surrounding hypoxia selectivity is based on the unique cellular trapping mechanism proposed for Cu(ATSM)⁴⁹. This copper(II) complex has been widely exploited *in vitro* and *in vivo*, due to its enhanced accumulation in hypoxic tissues. Generally, complexes with reduction potential more electronegative than -0.57 V vs. Ag/AgCl, display optimum hypoxia selectivity. Upon reduction, under hypoxia, these copper(II) complexes will partially dissociate into an intermediary copper(I) compound, which is more labile and eventually undergoes complete dissociation, liberating the free ligand⁵⁰. Copper(I) is then bound to specific binding proteins and chaperones such as Ctr1 and Atx1, respectively, which mediate the copper cellular pool⁵⁰. Whilst, under normoxia, the intermediary copper(I) compound will be reversibly oxidized to its copper(II) counterpart and diffuse out of the cells. Although the redox-properties provide reliable gold-standard in hypoxia selectivity, other factors influencing reduction rate should not be ruled out. Indeed, the degree of expression of intracellular reductases has shown to influence dissociation, as

well as other biological reductants such as ascorbate, thiols or NADP(H), as discussed previously.

TPZ's limited diffusion and incapacity to reach the relevant hypoxic cells, in tumor models have been previously reported^{26, 31, 36-39}. To overcome these limitations, analogues with increased lipophilicity (due to removal of H-bond donor of the 3NH₂ group), comparable to that of Cu(TPZ)₂, showed pronounced uptake, selectivity and tissue diffusion,^{26, 38, 43}. In agreement with these studies, the superior potency of the complex in C4-2B spheroids, compared to free TPZ, as confirmed by cell viability and cell cycle analysis, could be attributed to the high lipophilicity of the complex in combination with its good pH and serum stability, slow metabolism, and high electronegative potential (-0.75 V), resulting in decreased early onset toxicity to the outer layer of the spheroid and possible free ligand back-diffusion from the inner spheroid to induce high cell toxicity throughout the spheroid environment⁵¹. Furthermore, its higher DNA binding as we demonstrated, and reported by others²¹ could contribute to higher potency. However, the exact mechanism of toxicity in spheroids has yet to be investigated.

Conclusions

We successfully presented the synthesis and extensive characterization of a nano-sized Cu(TPZ)₂ complex that improved on TPZ's physicochemical properties and its hypoxia selectivity in PC. The synthesized copper-complex, exhibited high LogP, increased biocompatible redox-potential, slow metabolism, and high DNA binding, compared to TPZ. The intrinsic fluorescence of the complex enabled studying its cellular uptake, concluding on its significant hypoxia selective uptake and accumulation in the perinuclear area and in intracellular vesicles. In addition, our results reported for the first time the biological activity of Cu(TPZ)₂ complex in 3D hypoxia models. Interestingly, Cu(TPZ)₂ complex exhibited excellent hypoxia selectivity compared to TPZ, particularly in the castrate-resistant C4-2B PC monolayers. Furthermore, the improved structural activity of the complex correlated well with its enhanced efficacy in C4-2B spheroids. Further studies are still warranted to determine the Cu(TPZ)₂ exact mechanism of action *in vitro*. Finally, the limited solubility of the complex could be overcome using clinically relevant delivery systems, such as liposomes, to assess its therapeutic efficacy *in vivo*.

Conflicts of interest

There are no conflicts to declare.

Acknowledgements

Dr Al-Jamal is thankful for Prostate Cancer UK (CDF-12-002 Career Development Fellowship), and the Engineering and Physical Sciences Research Council (EPSRC) (EP/M008657/1) for their financial support; and the EPSRC UK National Mass Spectrometry Facility at Swansea University for the mass spectrometry analysis. Ms Vera Silva is grateful for The University of East Anglia (UEA)/School of Pharmacy, for funding her PhD study (studentship ref. 100099479).

References

- View Article Online
DOI: 10.1039/C9BM01905G
- Denny, W. A., The role of hypoxia-activated prodrugs in cancer therapy. *The Lancet. Oncology* **2000**, *1* (1), 25-29.
 - Guise, C. P.; Mowday, A. M.; Ashoorzadeh, A.; Yuan, R.; Lin, W. H.; Wu, D. H.; Smail, J. B.; Patterson, A. V.; Ding, K., Bioreductive prodrugs as cancer therapeutics: targeting tumor hypoxia. *Chinese journal of cancer* **2014**, *33* (2), 80-86.
 - Brown, J. M., SR 4233 (tirapazamine): a new anticancer drug exploiting hypoxia in solid tumours. *British journal of cancer* **1993**, *67* (6), 1163-1170.
 - Marcu, L.; Olver, I., Tirapazamine: from bench to clinical trials. *Current clinical pharmacology* **2006**, *1* (1), 71-79.
 - Reddy, S. B.; Williamson, S. K., Tirapazamine: a novel agent targeting hypoxic tumor cells. *Expert opinion on investigational drugs* **2009**, *18* (1), 77-87.
 - Kate, A. N.; Kumbhar, A. A.; Khan, A. A.; Joshi, P. V.; Puranik, V. G., Monitoring Cellular Uptake and Cytotoxicity of Copper(II) Complex Using a Fluorescent Anthracene Thiosemicarbazone Ligand. *Bioconjugate Chemistry* **2014**, *25* (1), 102-114.
 - L. J. Dearling, J.; J. Blower, P., Redox-active metal complexes for imaging hypoxic tissues: structure-activity relationships in copper(II) bis(thiosemicarbazone) complexes. *Chem Comm* **1998**, (22), 2531-2532.
 - Bergamo, A.; Dyson, P. J.; Sava, G., The mechanism of tumour cell death by metal-based anticancer drugs is not only a matter of DNA interactions. *Coord Chem Rev* **2018**, *360*, 17-33.
 - Blower, P. J.; Dilworth, J. R.; Maurer, R. I.; Mullen, G. D.; Reynolds, C. A.; Zheng, Y., Towards new transition metal-based hypoxic selective agents for therapy and imaging. *Journal of inorganic biochemistry* **2001**, *85* (1), 15-22.
 - Dearling, J. L.; Lewis, J. S.; Mullen, G. E.; Rae, M. T.; Zweit, J.; Blower, P. J., Design of hypoxia-targeting radiopharmaceuticals: selective uptake of copper-64 complexes in hypoxic cells *in vitro*. *European journal of nuclear medicine* **1998**, *25* (7), 788-92.
 - Dearling, J. L.; Lewis, J. S.; Mullen, G. E.; Welch, M. J.; Blower, P. J., Copper bis(thiosemicarbazone) complexes as hypoxia imaging agents: structure-activity relationships. *Journal of biological inorganic chemistry : JBIC : a publication of the Society of Biological Inorganic Chemistry* **2002**, *7* (3), 249-59.
 - Santini, C.; Pellei, M.; Gandini, V.; Porchia, M.; Tisato, F.; Marzano, C., Advances in copper complexes as anticancer agents. *Chemical reviews* **2014**, *114* (1), 815-62.
 - Knight, J. C.; Wuest, M.; Saad, F. A.; Wang, M.; Chapman, D. W.; Jans, H. S.; Lapi, S. E.; Kariuki, B. M.; Amoroso, A. J.; Wuest, F., Synthesis, characterisation and evaluation of a novel copper-64 complex with selective uptake in EMT-6 cells under hypoxic conditions. *Dalton Trans* **2013**, *42* (33), 12005-14.
 - Palanimuthu, D.; Shinde, S. V.; Somasundaram, K.; Samuelson, A. G., In Vitro and in Vivo Anticancer Activity of Copper Bis(thiosemicarbazone) Complexes. *J Med Chem* **2013**, *56* (3), 722-734.
 - Price, K. A.; Crouch, P. J.; Volitakis, I.; Paterson, B. M.; Lim, S.; Donnelly, P. S.; White, A. R., Mechanisms controlling the cellular accumulation of copper bis(thiosemicarbazonato) complexes. *Inorganic chemistry* **2011**, *50* (19), 9594-605.
 - Sandhaus, S.; Taylor, R.; Edwards, T.; Huddleston, A.; Wooten, Y.; Venkatraman, R.; Weber, R. T.; González-Sarrías, A.; Martin, P. M.; Cagle, P.; Tse-Dinh, Y.-C.; Beebe, S. J.; Seeram, N.; Holder, A. A., A novel copper(II) complex identified as a potent drug against colorectal and breast cancer cells and as a poison inhibitor for human topoisomerase IIα. *Inorg Chem Comm* **2016**, *64*, 45-49.
 - Zhang, Z.; Bi, C.; Schmitt, S. M.; Fan, Y.; Dong, L.; Zuo, J.; Dou, Q. P., 1,10-Phenanthroline promotes copper complexes into tumor cells and induces apoptosis by inhibiting the proteasome activity. *Journal of biological inorganic chemistry : JBIC : a publication of the Society of Biological Inorganic Chemistry* **2012**, *17* (8), 1257-67.
 - Adsule, S.; Barve, V.; Chen, D.; Ahmed, F.; Dou, Q. P.; Padhye, S.; Sarkar, F. H., Novel Schiff Base Copper Complexes of Quinoline-2 Carboxaldehyde as Proteasome Inhibitors in Human Prostate Cancer Cells. *J Med Chem* **2006**, *49* (24), 7242-7246.
 - Tardito, S.; Isella, C.; Medico, E.; Marchio, L.; Bevilacqua, E.; Hatzoglou, M.; Bussolati, O.; Franchi-Gazzola, R., The thioxotriazole copper(II) complex A0 induces endoplasmic reticulum stress and paraptotic death in human cancer cells. *The Journal of biological chemistry* **2009**, *284* (36), 24306-19.
 - Stefani, C.; Al-Eisawi, Z.; Jansson, P. J.; Kalinowski, D. S.; Richardson, D. R., Identification of differential anti-neoplastic activity of copper bis(thiosemicarbazones) that is mediated by intracellular reactive oxygen species generation and lysosomal membrane permeabilization. *Journal of inorganic biochemistry* **2015**, *152* (Supplement C), 20-37.
 - Lin, P.-S.; Ho, K.-C., New cytotoxic mechanism of the bioreductive agent Tirapazamine (SR 4233) mediated by forming complex with copper. *Radiation Oncology Investigations* **1996**, *4* (5), 211-220.
 - Lin, P. S.; Ho, K. C., CuTira brachytherapy: a new combination of radioactive copper isotopes and the hypoxic cytotoxin, tirapazamine, for targeted tumor

- therapy. *Journal of nuclear medicine : official publication, Society of Nuclear Medicine* **1998**, *39* (4), 677-8.
23. Sciences, E. L., ROS-ID® Hypoxia/Oxidative Stress Detection Kit. In *Product Manual*.
24. Walzl, A.; Unger, C.; Kramer, N.; Unterleuthner, D.; Scherzer, M.; Hengstschlager, M.; Schwanzler-Pfeiffer, D.; Dolznig, H., The Resazurin Reduction Assay Can Distinguish Cytotoxic from Cytostatic Compounds in Spheroid Screening Assays. *Journal of biomolecular screening* **2014**, *19* (7), 1047-59.
25. Meenongwa, A.; Brissos, R. F.; Soikum, C.; Chaveerach, P.; Gamez, P.; Trongpanich, Y.; Chaveerach, U., DNA-interacting and biological properties of copper(II) complexes from amidino-O-methylurea. *New Journal of Chemistry* **2015**, *39* (1), 664-675.
26. Hicks, K. O.; Siim, B. G.; Jaiswal, J. K.; Pruijn, F. B.; Fraser, A. M.; Patel, R.; Hogg, A.; Liyanage, H. D.; Dorie, M. J.; Brown, J. M.; Denny, W. A.; Hay, M. P.; Wilson, W. R., Pharmacokinetic/pharmacodynamic modeling identifies SN30000 and SN29751 as tirapazamine analogues with improved tissue penetration and hypoxic cell killing in tumors. *Clinical cancer research : an official journal of the American Association for Cancer Research* **2010**, *16* (20), 4946-57.
27. Dux, E. L. The Development Of Transition Metal Complexes To Target Hypoxic Cells. Doctoral Thesis, University of York, 2011.
28. Ko, K. C.; Wu, J.-S.; Kim, H. J.; Kwon, P. S.; Kim, J. W.; Bartsch, R. A.; Lee, J. Y.; Kim, J. S., Rationally designed fluorescence 'turn-on' sensor for Cu²⁺. *Chem Comm* **2011**, *47* (11), 3165-3167.
29. Valderrama-Negrón, A. C.; Alves, W. A.; Cruz, Á. S.; Rogero, S. O.; de Oliveira Silva, D., Synthesis, spectroscopic characterization and radiosensitizing properties of acetato-bridged copper(II) complexes with 5-nitroimidazole drugs. *Inorganica Chimica Acta* **2011**, *367* (1), 85-92.
30. Poole, J. S.; Hadad, C. M.; Platz, M. S.; Fredin, Z. P.; Pickard, L.; Guerrero, E. L.; Kessler, M.; Chowdhury, G.; Kotandeniya, D.; Gates, K. S., Photochemical electron transfer reactions of tirapazamine. *Photochemistry and photobiology* **2002**, *75* (4), 339-45.
31. Hicks, K. O.; Pruijn, F. B.; Sturman, J. R.; Denny, W. A.; Wilson, W. R., Multicellular resistance to tirapazamine is due to restricted extravascular transport: a pharmacokinetic/pharmacodynamic study in HT29 multicellular layer cultures. *Cancer research* **2003**, *63* (18), 5970-7.
32. Zagorevskii, D.; Song, M.; Breneman, C.; Yuan, Y.; Fuchs, T.; Gates, K. S.; Greenleaf, C. M., A mass spectrometry study of tirapazamine and its metabolites: Insights into the mechanism of metabolic transformations and the characterization of reaction intermediates. *J Am Chem Soc Mass Spec* **2003**, *14* (8), 881-892.
33. Birincioglu, M.; Jaruga, P.; Chowdhury, G.; Rodriguez, H.; Dizdaroglu, M.; Gates, K. S., DNA Base Damage by the Antitumor Agent 3-Amino-1,2,4-benzotriazine 1,4-Dioxide (Tirapazamine). *Journal of the American Chemical Society* **2003**, *125* (38), 11607-11615.
34. Lin, D. L.; Tarnowski, C. P.; Zhang, J.; Dai, J.; Rohn, E.; Patel, A. H.; Morris, M. D.; Keller, E. T., Bone metastatic LNCaP-derivative C4-2B prostate cancer cell line mineralizes in vitro. *The Prostate* **2001**, *47* (3), 212-221.
35. Higgins, L. H.; Withers, H. G.; Garbens, A.; Love, H. D.; Magnoni, L.; Hayward, S. W.; Moyes, C. D., Hypoxia and the metabolic phenotype of prostate cancer cells. *Biochimica et biophysica acta* **2009**, *1787* (12), 1433-43.
36. Durand, R. E.; Olive, P. L., Evaluation of bioreductive drugs in multicell spheroids. *International journal of radiation oncology, biology, physics* **1992**, *22* (4), 689-92.
37. Hicks, K. O.; Fleming, Y.; Siim, B. G.; Koch, C. J.; Wilson, W. R., Extravascular diffusion of tirapazamine: effect of metabolic consumption assessed using the multicellular layer model. *International journal of radiation oncology, biology, physics* **1998**, *42* (3), 641-649.
38. Monge, A.; Palop, J. A.; de Cerain, A. L.; Senador, V.; Martínez, F. J.; Sainz, Y.; Narro, S.; Garcia, E.; de Miguel, C., Hypoxia-Selective Agents Derived from Quinoxaline 1,4-Di-N-oxides. *J Med Chem* **1995**, *38* (10), 1786-1792.
39. Kyle, A. H.; Minchinton, A. I., Measurement of delivery and metabolism of tirapazamine to tumour tissue using the multilayered cell culture model. *Cancer Chemotherapy and Pharmacology* **1999**, *43* (3), 213-220.
40. Wouters, B. G.; Delahoussaye, Y. M.; Evans, J. W.; Birrell, G. W.; Dorie, M. J.; Wang, J.; MacDermed, D.; Chiu, R. K.; Brown, J. M., Mitochondrial Dysfunction after Aerobic Exposure to the Hypoxic Cytotoxin Tirapazamine. *Cancer research* **2001**, *61* (1), 145-152.
41. Delahoussaye, Y. M.; Hay, M. P.; Pruijn, F. B.; Denny, W. A.; Brown, J. M., Improved potency of the hypoxic cytotoxin tirapazamine by DNA-targeting. *Biochemical pharmacology* **2003**, *65* (11), 1807-15.
42. Kathiresan, S.; Muges, S.; Murugan, M.; Ahamed, F.; Annaraj, J., Mixed-ligand copper(II)-phenolate complexes: structure and studies on DNA/protein binding profiles, DNA cleavage, molecular docking and cytotoxicity. *RSC Advances* **2016**, *6* (3), 1810-1825.
43. Hay, M. P.; Gamage, S. A.; Kovacs, M. S.; Pruijn, F. B.; Anderson, R. F.; Patterson, A. V.; Wilson, W. R.; Brown, J. M.; Denny, W. A., Structure-activity relationships of 1,2,4-benzotriazine 1,4-dioxides as hypoxia-selective analogues of tirapazamine. *J Med Chem* **2003**, *46* (1), 169-82.
44. Torre, M. H.; Gambino, D.; Araujo, J.; Cerecetto, H.; Gonzalez, M.; Lavaggi, M. L.; Azqueta, A.; Lopez de Cerain, A.; Vega, A. M.; Abram, U.; Costa-Filho, A. J., Novel Cu(II) quinoxaline N1,N4-dioxide complexes as selective hypoxic cytotoxins. *European journal of medicinal chemistry* **2005**, *40* (5), 473-80.
45. Urquiola, C.; Gambino, D.; Cabrera, M.; Lavaggi, M. L.; Cerecetto, H.; González, M.; de Cerain, A. L.; Monge, A.; Costa-Filho, A. J.; Torre, M. H., New copper-based complexes with quinoxaline N1,N4-dioxide derivatives, potential antitumoral agents. *Journal of inorganic biochemistry* **2008**, *102* (1), 119-126.
46. Skarsgard, L. D.; Skwarchuk, M. W.; Vinczan, A.; Chaplin, D. J., The effect of pH on the aerobic and hypoxic cytotoxicity of SR4233 in HT-29 cells. *British journal of cancer* **1993**, *68* (4), 681-3.
47. Kheirloomoom, A.; Mahakian, L. M.; Lai, C.-Y.; Lindfors, H. A.; Seo, J. W.; Paoli, E. E.; Watson, K. D.; Haynam, E. M.; Ingham, E. S.; Xing, L.; Cheng, R. H.; Borowsky, A. D.; Cardiff, R. D.; Ferrara, K. W., Copper-doxorubicin as a nanoparticle cargo retains efficacy with minimal toxicity. *Mol pharm* **2010**, *7* (6), 1948-1958.
48. Delahoussaye, Y. M.; Evans, J. W.; Brown, J. M., Metabolism of tirapazamine by multiple reductases in the nucleus. *Biochemical pharmacology* **2001**, *62* (9), 1201-9.
49. Holland, J. P.; Lewis, J. S.; Dehdashti, F., Assessing tumor hypoxia by positron emission tomography with Cu-ATSM. *Q J Nucl Med Mol Imaging* **2009**, *53* (2), 193-200.
50. Xiao, Z.; Donnelly, P. S.; Zimmermann, M.; Wedd, A. G., Transfer of copper between bis(thiosemicarbazone) ligands and intracellular copper-binding proteins. insights into mechanisms of copper uptake and hypoxia selectivity. *Inorganic chemistry* **2008**, *47* (10), 4338-47.
51. Wilson, W. R.; Moselen, J. W.; Cliffe, S.; Denny, W. A.; Ware, D. C., Exploiting tumor hypoxia through bioreductive release of diffusible cytotoxins: The cobalt(III)-nitrogen mustard complex SN 24771. *International journal of radiation oncology, biology, physics* **1994**, *29* (2), 323-327.

Figures and captions

View Article Online
DOI: 10.1039/C9BM01905G

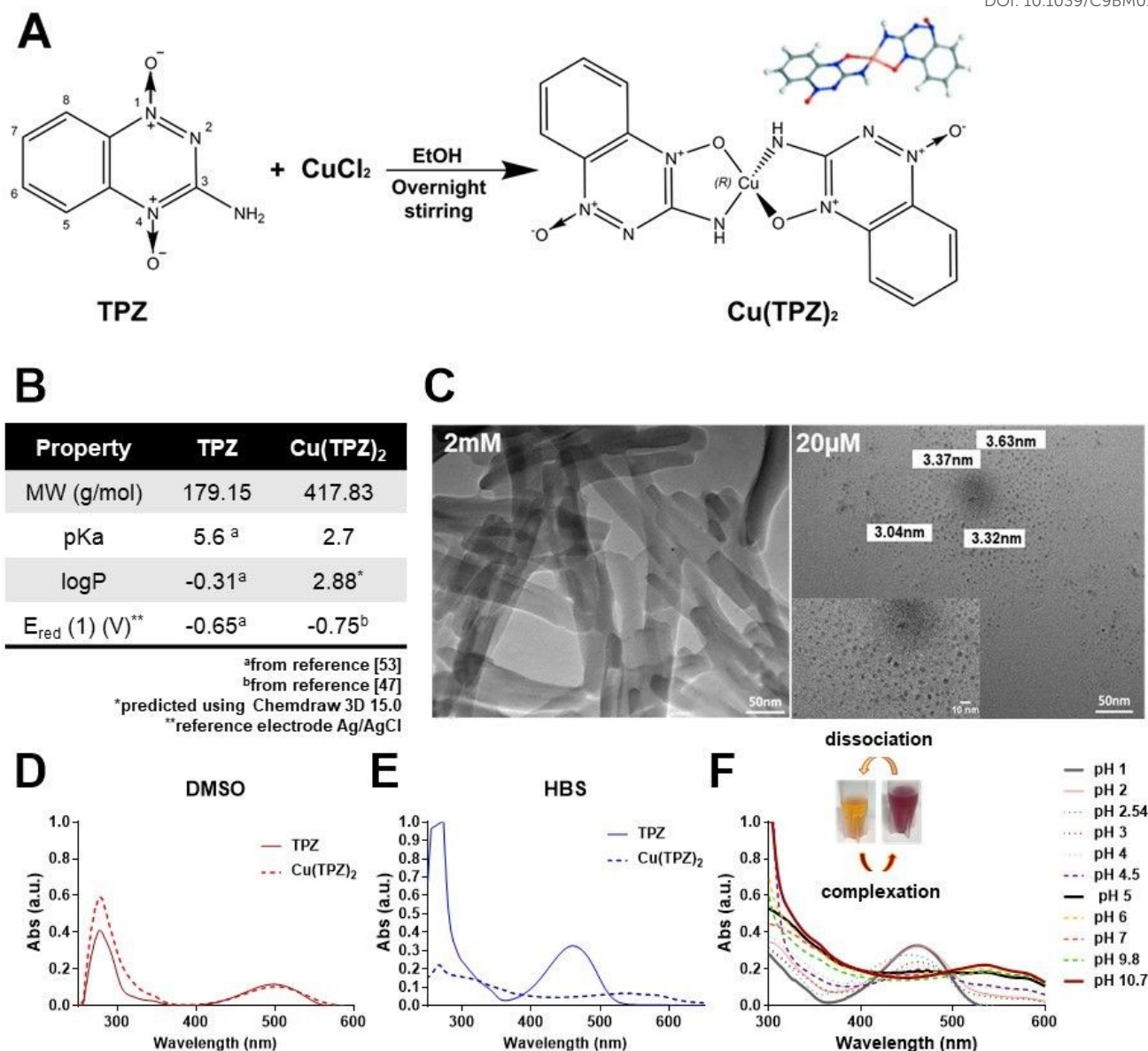


Figure 1. Synthesis and characterization of hypoxia-selective Cu(TPZ)₂ complex. A) Schematic representation of the synthesis protocol of Cu(TPZ)₂ complex in ethanol (Inset: optimised structure); B) A summary of main physicochemical properties of TPZ and Cu(TPZ)₂; C) TEM images of Cu(TPZ)₂ at high (2 mM) and low (20 μM) concentrations, depicting a concentration-dependent, self-aggregation of the complex in ethanol; D) Absorbance spectra of TPZ (10 μM, solid line) and Cu(TPZ)₂ (5 μM, dotted line) in DMSO; E) Absorbance spectra of TPZ (60 μM, solid line) and Cu(TPZ)₂ (30 μM, dotted line) in HBS; and F) Absorbance of Cu(TPZ)₂ (50 μM) at different pH values, illustrating a pH-dependent dissociation of Cu(TPZ)₂. Inset shows a yellow color change of TPZ to a dark red solution upon complexation and vice-versa, upon dissociation.

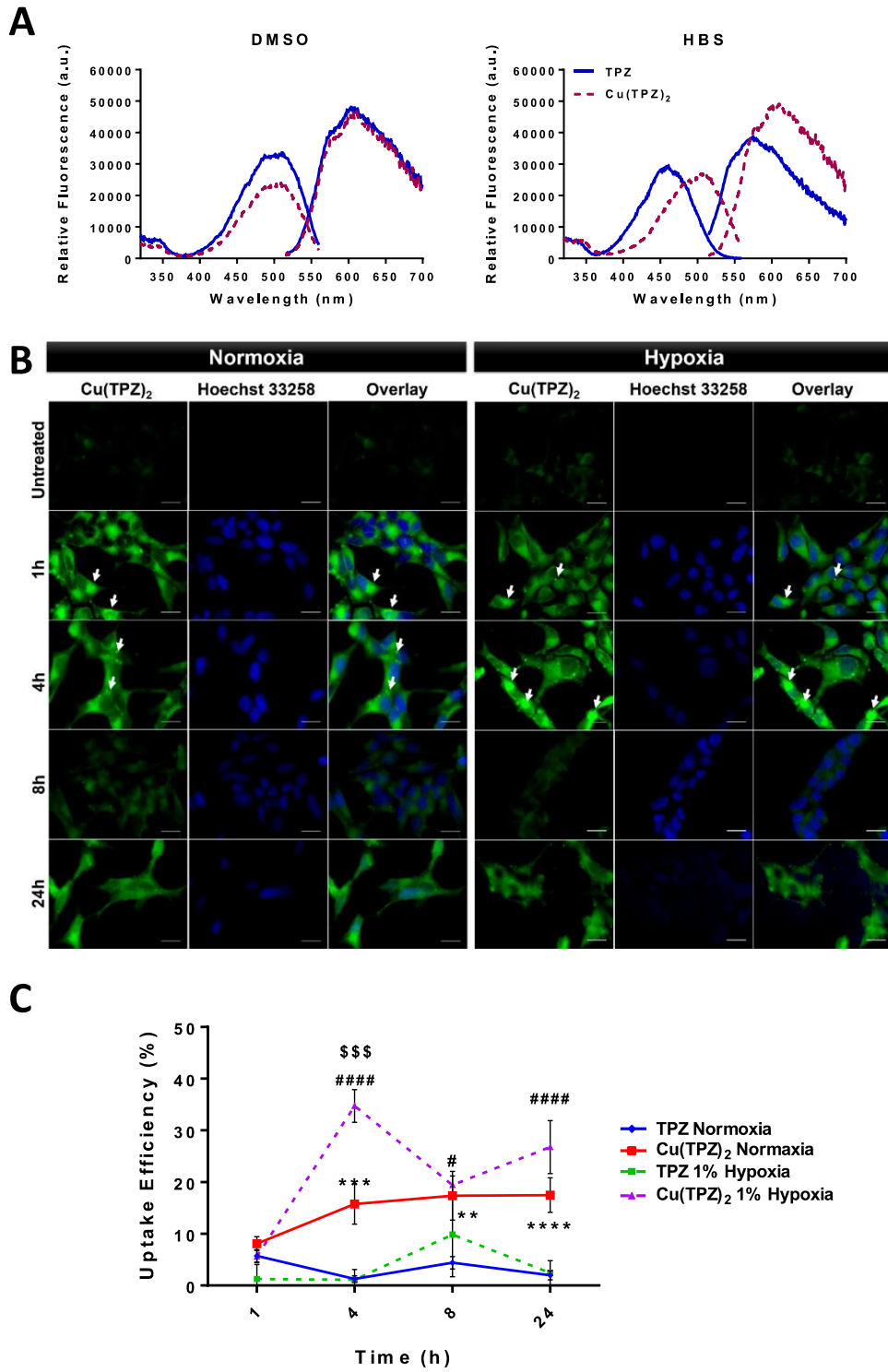


Figure 2. Intrinsic fluorescence, uptake and cellular localization of Cu(TPZ)₂ complex in C4-2B prostate cancer cells. A) Fluorescence spectra of TPZ and Cu(TPZ)₂ diluted in DMSO (left) and HBS (right) (DMSO: $\lambda_{exc}/\lambda_{em}$ 490/600 nm, HBS: $\lambda_{exc}/\lambda_{em}$ 450/570 nm (TPZ) and $\lambda_{exc}/\lambda_{em}$ 500/600 nm (Cu(TPZ)₂). B) Qualitative uptake of Cu(TPZ)₂ (100 μ M equivalent TPZ) at 1, 4, 8 and 24 h under normoxia and 1% hypoxia. The white arrows depict intense green puncta signals, suggesting accumulation of the complex in intracellular vesicles. The signals were more prominent under hypoxic conditions and in the perinuclear area. Images are representative of at least 50 cells of two independent experiments (n=2). Green channel: Cu(TPZ)₂ treated cells; Blue channel: nuclei stained with Hoechst 33258. Scale bars, 20 μ m. C) Quantitative uptake of TPZ and Cu(TPZ)₂ in C4-2B cells. Cells were incubated with 25 μ M equivalent TPZ, and the cellular uptake was determined at 1, 4, 8 and 24 h under normoxia and 1% hypoxia. Fluorescence was measured at $\lambda_{exc}/\lambda_{em}$ 485/590 nm in DMSO. Results were expressed as mean \pm SD for triplicates of three independent experiments (n=3). Statistical analysis using Two-way ANOVA multiple comparison with Bonferroni Post-test (GraphPad Prism version 7.0, GraphPad Software Inc., La Jolla, CA, USA) was performed to compare uptake of TPZ vs Cu(TPZ)₂: (**p \leq 0.01, ***p \leq 0.001 and ****p \leq 0.0001, comparing drugs under normoxia; #p \leq 0.05, and ###p \leq 0.0001, comparing drugs under hypoxia; and \$\$\$p \leq 0.001, comparing Cu(TPZ)₂ under hypoxia and normoxia).

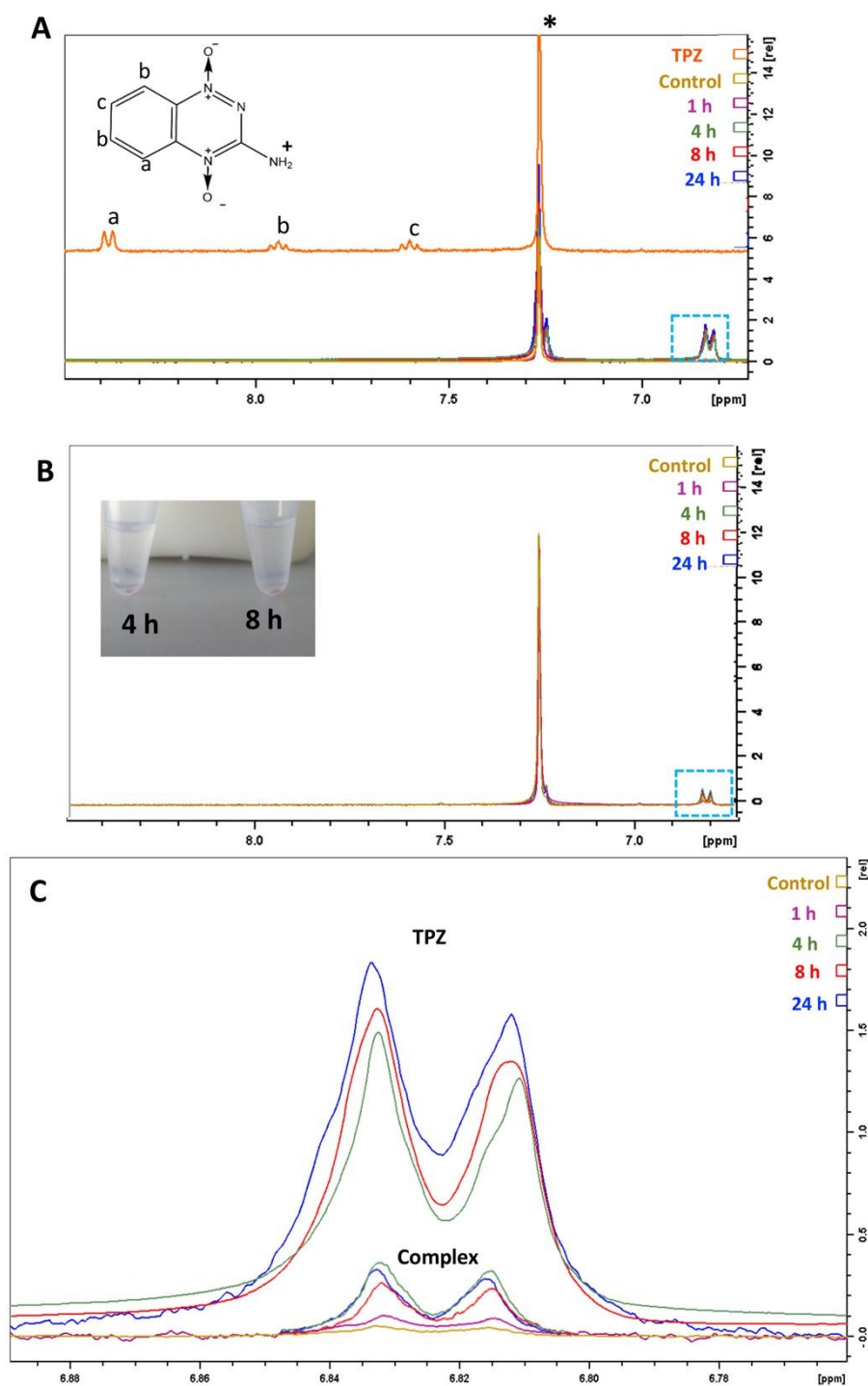


Figure 3: ¹H-NMR in CDCl₃ of C4-2B cell lysates. Cells were incubated under 1% hypoxia with (A) TPZ and (B) Cu(TPZ)₂ for different duration (1, 4, 8, 24 h). Untreated cells were used as a control. Samples were prepared for NMR analysis as described in the methods section. TPZ (1 mg/ 400 µl) was also analysed (peaks a,b,c), however the complex was not soluble in CDCl₃ and no peaks were detected. The photograph (inset in Figure. 3B) represents the pinkish cell lysate pellets, indicating the presence of Cu(TPZ)₂ in the cell lysate samples. The main sharp peak (*) represents the solvent. (C) peak heights for the TPZ and Cu(TPZ)₂ metabolites.

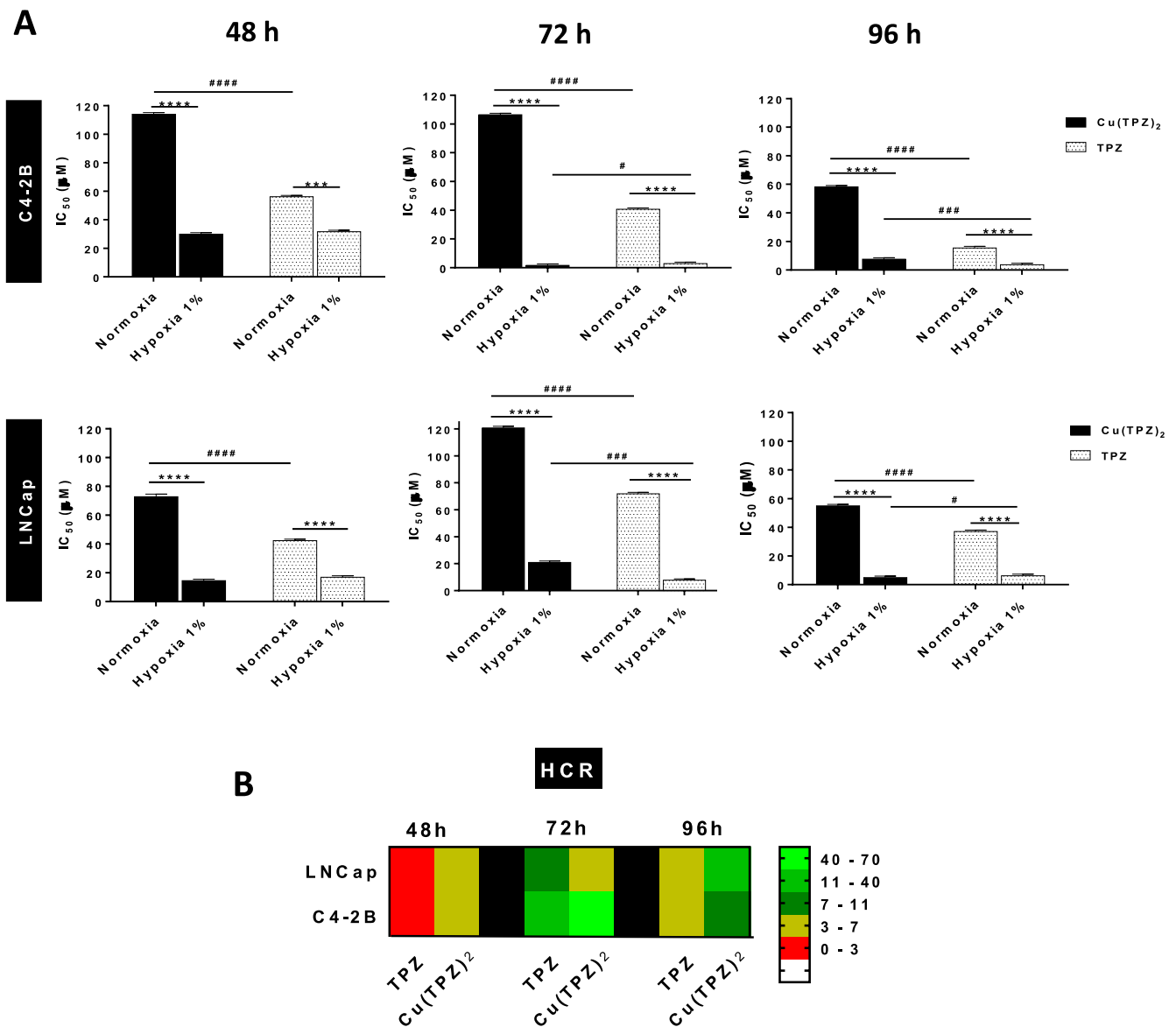


Figure 4. IC₅₀ values of Cu(TPZ)₂ complex and TPZ incubated with two PCa cells under normoxia and 1% hypoxia. A) C4-2B (top panel) and LNCap (bottom panel) cells were incubated under normoxia and 1% hypoxia with equivalent doses of Cu(TPZ)₂ and TPZ, and IC₅₀ values were determined after 48, 72 and 96 h of incubation; B) Heat map of the hypoxia cytotoxicity ratio (HCR) values obtained for TPZ and Cu(TPZ)₂ in the two PCa cell lines studied above. The IC₅₀ values for inhibition were assessed by the resazurin assay and determined by nonlinear regression analysis of the data fit to a four-parameter equation (GraphPad Prism version 7.0, GraphPad Software Inc., La Jolla, CA, USA) and used to calculate HCR: IC₅₀ normoxia/IC₅₀ hypoxia. Results are expressed as mean ± SD for six replicates of at least three independent experiments (n>3). Statistical analysis: Two-way ANOVA multiple comparison Bonferroni Post-hoc test (**p<0.001 and ****p<0.0001, comparing normoxia vs hypoxia; #p<0.05, ###p<0.001 and ####p<0.0001, comparing Cu(TPZ)₂ vs TPZ).

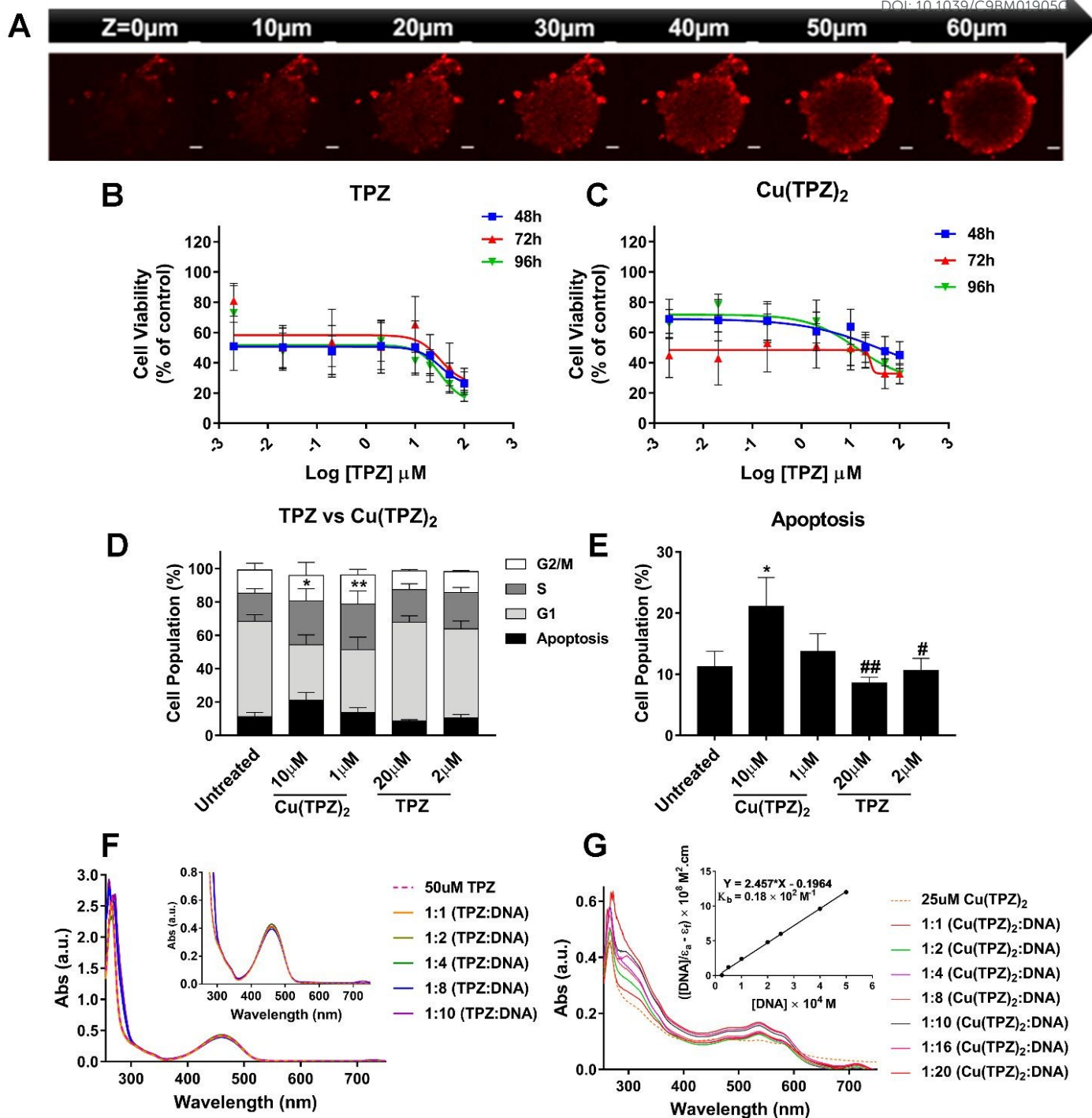


Figure 5. *In vitro* toxicity of Cu(TPZ)₂ in C4-2B spheroids and DNA binding assay. A) fluorescent images of 3D C4-2B spheroids (day 5) incubated with CYTO-ID[®] Hypoxia Detection probe (500 nM, Enzo Life Sciences, UK) for 4 h, taken using an inverted Zeiss Axiovert 200M with Texas Red (596/670 nm) filter and equipped with a Zeiss ApoTome (Carl Zeiss, UK) to create optical sections free of scattered light. For each spheroid, a Z-stack with 10 μm thickness was generated. Scale bar: 100 μm. IC₅₀ curves of B) TPZ and C) Cu(TPZ)₂ in C4-2B spheroids. 5 days post seeding, tumor spheroids were incubated with equivalent doses of Cu(TPZ)₂ and TPZ, and IC₅₀ values were determined after 48, 72 and 96 h. Cell viability was assessed by the resazurin assay, with spheroids pre-treated for 30 min with EDTA (5 mM). Results were normalized to untreated and expressed as mean ± SD for six replicates of at least two independent experiments (n≥2). The IC₅₀ values for inhibition were

determined by nonlinear regression analysis of the data fit to a four-parameter equation (GraphPad Prism version 7.0, GraphPad Software Inc., La Jolla, CA, USA). C4-2B spheroids were cultured for 5 days, then treated for 72 h with 20 and 2 μM equivalent TPZ in both free and complex forms and analyzed for D) cell cycle distribution and E) the percentage of apoptotic cells. Each flow cytometry plot depicts the mean \pm SD percentage of G1 (2n), S and G2/M (4n) fraction population. The data represents the mean of at least ten pooled spheroids of two independent experiments (n=2). F) Absorption spectra of the TPZ (50 μM) in the absence (dashed line) and presence (solid line) of increasing amounts of CT-DNA at room temperature in 5 mM Tris/HCl/50 mM NaCl buffer, PH 7.2. Inset shows a zoom in of the visible spectral region, showing no changes in the spectrum. G) Absorption spectra of the complex (25 μM) in the absence (dashed line) and presence (solid line) of increasing amounts of CT-DNA at room temperature in 5 mM Tris/HCl/50 mM NaCl buffer, pH 7.2. The arrow depicts the absorbance spectrum changes on increasing the CT-DNA concentration. Inset shows the plot of $[\text{DNA}]/(\epsilon_a - \epsilon_f) / (\epsilon_b - \epsilon_f)$ vs $[\text{DNA}]$ and derived K_b value (M^{-1}); Statistical analysis: Two-way ANOVA multiple comparison Bonferroni Post-hoc test (* $p < 0.05$ ** $p < 0.01$, compared to control and # $p < 0.05$ ## $p < 0.01$, comparing TPZ vs $\text{Cu}(\text{TPZ})_2$, GraphPad Prism version 7.0).

Table of Content

